

# Dynamical response of magnetic tubes to transverse perturbations

## II. Towards thin flux tubes

U. Ziegler and P. Ulmschneider

Institut für Theoretische Astrophysik der Universität Heidelberg, Tiergartenstr. 15, D-69121 Heidelberg, Germany

Received 20 May 1997 / Accepted 10 July 1997

**Abstract.** The dynamical response of magnetic flux tubes due to local transverse periodic perturbations is investigated by numerical means. Our aim was to check the applicability of the *thin* flux tube approximation for vertically oriented flux tubes with moderate magnetic field strength (plasma  $\beta = 1$ ) and diameters 100 km, 50 km and 25 km immersed in an otherwise homogeneous nonmagnetic environment. All tubes has been subject to the same driver. To resolve the flux tube in a  $2000 \times 2000 \times 1000$  km<sup>3</sup> computational domain, a multiple nested grid version of a 3D MHD code is used.

We find that a description as ideally *thin* flux tube becomes more and more questionable if the diameter of the tube decreases. For the thinnest tube we found eg. an almost complete split up into a fork-like geometry with two counterrotating legs. This can be explained by a more rigorous interaction of the tube with the ambient medium: Geometrically thinner flux tubes are less inert than corresponding thick tubes and therefore experience stronger backreaction forces because thinner tubes are easier to displace horizontally. As a consequence of this, their cross sections are significantly deformed contradictory to the assumptions made in the *thin* flux tube approximation. The energy loss from the internal tube motions to the surroundings by acoustic radiation is found to be anticorrelated with the tube radius ie. thinner tubes loose more wave energy than thicker ones.

**Key words:** MHD – Sun: magnetic fields – magnetic fields

### 1. Introduction

Due to its mathematical simplicity, the so called *thin* (or *slender*) flux tube approximation referred shortly as TFA has gained a great popularity in modelling the dynamics of magnetic flux concentrations. In this approximation, flux tubes are thought of as essentially one-dimensional objects which do not possess much structure perpendicular to their characterizing axis. In a

very simple picture, a *thin* flux tube may be considered as a sequence of individual mass elements which mutually communicate via hydrodynamic forces and the Lorentz force.

What are the criteria that a flux tube can be regarded as *thin*? Intuitively, one would propose geometrically thin flux tubes as promising candidates. By definition, in these tubes the local radius  $R_0$  is much smaller than the length scale  $L_0$  at which variations along the tube occur.  $L_0$  may be given by the scale-height of the temperature or pressure profile if the flux tube is embedded in a stratified atmosphere, or by the wavelength of a disturbance propagating along the flux tube. Defining a thickness parameter  $\alpha = R_0/L_0$ , the criterion for a thin flux tube may be formulated as  $\alpha \ll 1$ .

Generally,  $\alpha \ll 1$  is not a sufficient condition for the applicability of the TFA. This can be seen as follows. The fundamental variables  $\rho, p, e, \mathbf{v}$  and  $\mathbf{B}$  (notation as usual) may be expanded into a Taylor series perpendicular to the tube axis according to

$$f(s, x, y) = f_0(s) + x f_{10}(s) + y f_{01}(s) + \frac{1}{2} x^2 f_{20}(s) + \frac{1}{2} y^2 f_{02}(s) + xy f_{11}(s) + \dots \quad (1)$$

Here,  $f$  stands for any of the variables just mentioned.  $f_0$  denotes its value on the tube axis.  $f_{ij}(s) = \partial^{i+j} f / \partial x^i \partial y^j |_{axis}$  and higher-order derivatives are indicated by dots. The tube axis is characterized by the arc-length  $s$  measured from an arbitrary starting point  $s_0$ .  $(x, y)$  are Cartesian coordinates perpendicular to the axis in a local frame given by the tangential, normal, and binormal unit vectors of the curve (Fig. 1). Of course, the uniqueness of the coordinate set  $(s, x, y)$  should be guaranteed excluding eg. the possibility of reconnection phenomena in which flux tube sections with opposite field orientation collide.

With the help of Eq. (1), the very complicated 3D problem can be reduced to the 1D problem in the TFA. The fundamental variables are then replaced by its ‘moments’  $f_0(s)$  and  $f_{ij}(s)$  up to certain but small order  $i+j$ . If the expansion written down for  $\rho, p, e, \mathbf{v}$  and  $\mathbf{B}$  is inserted into the MHD equations (transformed to the coordinates  $(s, x, y)$ ), one formally ends up with a set of equations for the respective order of approximation. Thus, the problem (the environment of the flux tube is excluded for the

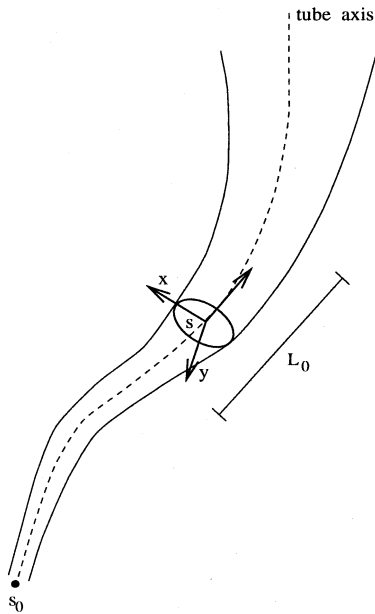


**Fig. 1.** The local frame of reference at arc-length  $s$  measured from a starting point  $s_0$ .

moment) no longer depends on all space coordinates but only on the parameter  $s$  at the expense of an increase in the number of variables, namely the moments. Of course, this procedure only makes sense if higher-order terms in the expansion can be neglected.

The TFA supposes that cross-sectional variations are small ie.  $R_0 |\nabla_{\perp} f| \ll |f_0|$ , where  $\nabla_{\perp}$  is the transverse part of the gradient. The longitudinal length scale  $L_0$  may be defined by  $L_0 = |f_0 / \partial_s f|$ , where  $\partial_s$  denotes the derivative in direction of the tube axis. Eliminating  $f_0$  yields as sufficient condition for the applicability of the TFA:

$$\frac{R_0}{L_0} \left| \frac{\nabla_{\perp} f}{\partial_s f} \right| \ll 1. \quad (2)$$

Defining  $\delta = |\nabla_{\perp} f| / |\partial_s f|$ , this inequality can be written as  $\alpha \delta \ll 1$ . If  $\delta \lesssim 1$ , the condition simply reduces to  $\alpha \ll 1$ . If, however,  $\delta \gg 1$  ie.  $|\nabla_{\perp} f| \gg |\partial_s f|$ , then  $\alpha \ll 1$  is not sufficient for the application of the TFA. Thus, geometrically thin flux tubes ( $\alpha \ll 1$ ) may not be *thin* in the sense of the TFA violating condition (2). On the other hand, thick tubes ( $\alpha \gtrsim 1$ ) may be describable within this theory, if  $\delta \ll 1$  ie. transverse gradients are relatively small compared to longitudinal ones.

The TFA concept has only been worked out in cases with various degrees of simplifications. This is because first the general transformation of the MHD equations to the new variables  $(s, x, y)$  is not easy to perform: Inertial forces appropriate for the local coordinate system have to be added and the time-dependence of the arbitrarily chosen  $s_0$ , fixed eg. at a fluid element, must be described. Second, the resulting moment equations are not closed because eg. of the artificial exclusion of the environment. One needs a closure relation in addition. Usually, the moment equations are complemented by a prescribed

time-independent external pressure function which relates the behaviour of the tube plasma to that of the ambient gas by demanding instantaneous pressure equilibrium at the tube surface.

The governing equations of the so-called *traditional* (zeroth-order) thin flux tube approximation (TTFA) are derived formally by taking the limit  $\alpha \delta \rightarrow 0$ . This corresponds to the simple picture of stacked mass elements mentioned earlier. The TTFA has been applied in numerous investigations to study the nonlinear propagation of transverse waves (Roberts & Webb 1978, Spruit 1981ab, Choudhuri 1990, Ulmschneider et al. 1991, Cheng 1992, Schramkowski & Achterberg 1993, Fan et al. 1994, Moreno-Insertis et al. 1996, Osin et al. 1997). Actually, it has been used up to geometrical thickness  $\alpha \approx 1$  and more. In the way the TTFA is constructed mathematically, however, their application is dubious in this case. Indeed, in Ziegler & Ulmschneider (1997) hereafter referred to as Paper I it has been shown that the TTFA does not represent an accurate method for ‘thick’ tubes, if excited by transverse oscillations. Eg., thick tubes develop a nonaxisymmetric longitudinal wave-like motion not explainable within the framework of the TTFA.

For the special situation of vertically oriented axisymmetric flux tubes, Ferriz-Mas et al. (1989) have extended the TFA up to second order in the expansion. In this case, cylindrical Eulerian coordinates  $(z, R)$  can be used which due to symmetry properties considerably reduce the complexity because a lot of moments  $f_{ij}$  in (1) vanish as shown by Ferriz-Mas & Schüssler (1989). However, this approach is not able to describe the excitation of transverse waves in which we are interested, but is restricted to deal with longitudinal excitation.

The basic assumptions involved in the TFA are twofold. The first point is that cross-sectional variations are considered small so that higher-order moments can be neglected in the dynamical equations. The second important point concerns the interaction between the tube and the ambient medium not discussed so far. The assumption of pressure equilibrium at the tube surface may not be sufficient if the flux tube moves in a gaseous medium. Then, an external force taking into account the backreaction of the ambient medium has to be added. However, it is still not clarified with final certainty, how such a force term has to be incorporated even in the TTFA equations. In any case, it is assumed that the backreaction of the environment is moderate so that the cross section of the tube does not change significantly, thus, allowing an expansion of the form (1) with higher-order moments to be negligible.

It is our intention to shed more light on the applicability of the TFA for the special case of transversely and periodically perturbed cylindrical flux tubes viewed as 3D objects. We start our numerical investigation with a geometrically thick flux tube and move into the regime of geometrically thin tubes holding fixed the thermal and magnetic properties. In Paper I, we have studied the excitation of MHD waves in flux tubes of fixed dimension but with different magnetic field strength. We are now interested in the question to what extend the dynamics of wave propagation is influenced by the interaction between the flux tube and its ambient medium and whether a treatment within the theory of *thin* flux tubes can be justified or not. For this pur-

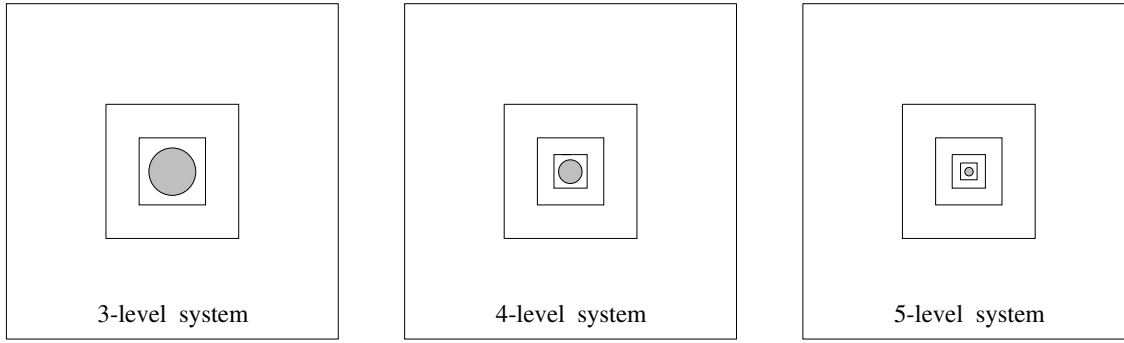


**Fig. 2.** Representation of the nesting of grids used in the numerical simulations. The 3–(4–,5–)level grid system is applied in the  $C_{50}$  ( $C_{25}$ ,  $C_{12.5}$ ) case. The flux tube cross section is illustrated as shaded area.

**Table 1.** Properties of the nested grid system.

level	domain [km]		# grid points	resolution [km]
basic	$-1000 < x, y < 1000$	$0 < z < 1000$	$100 \times 100 \times 50$	20
1	$-150 < x, y < 150$	$0 < z < 1000$	$30 \times 30 \times 100$	10
2	$-75 < x, y < 75$	$0 < z < 1000$	$30 \times 30 \times 200$	5
3	$-37.5 < x, y < 37.5$	$0 < z < 1000$	$30 \times 30 \times 400$	2.5
4	$-18.75 < x, y < 18.75$	$0 < z < 1000$	$30 \times 30 \times 800$	0.125

pose a multiple nested-grid 3D MHD computer code is used which takes into account both the flux tube and the surrounding medium.

As our fully time-dependent 3D simulations are extremely demanding in computer time our present work discusses only cases with moderate magnetic field strength, the so called  $\beta = 1$  cases. Here  $\beta = 8\pi p/B^2$  is the plasma  $\beta$ . Our conclusions on the applicability of the TFA given in Sect. 4 are therefore restricted to this case and may not apply to cases with  $\beta \gg 1$  or  $\beta \ll 1$ .

## 2. Numerical model

The general equations governing adiabatic flow in a perfectly conducting, inviscid gas permeated by a magnetic field are given by:

$$\frac{\partial \rho}{\partial t} + \nabla(\rho \mathbf{v}) = 0, \quad (3)$$

$$\frac{\partial(\rho \mathbf{v})}{\partial t} + \nabla(\rho \mathbf{v} \otimes \mathbf{v}) = -\nabla p - \nabla \left( \frac{\mathbf{B}^2}{8\pi} \right) + \frac{1}{4\pi} (\mathbf{B} \cdot \nabla) \mathbf{B}, \quad (4)$$

$$\frac{\partial e}{\partial t} + \nabla(e \mathbf{v}) = -p \nabla \mathbf{v}, \quad (5)$$

$$\frac{\partial \mathbf{B}}{\partial t} = \nabla \times (\mathbf{v} \times \mathbf{B}), \quad (6)$$

$$p = (\gamma - 1)e \quad (7)$$

$$\nabla \cdot \mathbf{B} = 0. \quad (8)$$

In the above equations  $\rho$ ,  $p$ ,  $e$ ,  $\mathbf{v}$ , and  $\mathbf{B}$  are the gas density, pressure, thermal energy density, velocity, and magnetic field, respectively.  $\gamma$  is the ratio of specific heats taken as 5/3. Note that the equation of motion (Eq. (4)) is written in a compact form

where  $\mathbf{v} \otimes \mathbf{v}$  denotes a dyad. These equations do not take into account physical processes such as radiation transfer, heat conduction or magnetic diffusivity which all may be more or less important in modelling the dynamics of magnetic structures in atmospheres of stars, galactic disks or accretion disks. In addition, gravity is ignored. Instead, a flux tube model is constructed analogous to that in Paper I suitable for the problem of wave propagation in a uniform cylinder of magnetic field embedded in a uniform nonmagnetic background medium. The tube axis is oriented in  $z$ -direction, referred to as vertical direction subsequently. The variables inside and outside the tube are denoted by subscripts ‘0’ and ‘e’, respectively.

The horizontal component of the equation of motion (with  $\mathbf{v} = 0$ ,  $\partial/\partial t \equiv 0$ ) leads to

$$p_e = p_0 + \frac{B_{z,0}^2}{8\pi} \quad (9)$$

which balances the external pressure  $p_e$  and the total (gas + magnetic) pressure inside the tube. Introducing  $\beta$ , Eq. (9) can also be expressed in the form

$$\frac{p_0}{p_e} = \left( 1 + \frac{1}{\beta} \right)^{-1} \quad (10)$$

which relates the ratio of gas pressures with the plasma  $\beta$ . The surrounding gas and tube plasma is taken to be isothermal initially ie.  $p_e/\rho_e = p_0/\rho_0$ , so that

$$\frac{\rho_0}{\rho_e} = \left( 1 + \frac{1}{\beta} \right)^{-1}. \quad (11)$$

Throughout the calculations, we assume  $\beta = 1$ . To have a concrete situation in mind we specify external values  $\rho_e =$

$1.95 \cdot 10^{-7} \text{ g/cm}^3$  and  $p_e = 1.17 \cdot 10^5 \text{ dyn/cm}^2$  taken from model calculations of the solar atmosphere (Vernazza et al. 1981). From Eqs. (10) and (11) the internal gas density and gas pressure is derived. One obtains  $\rho_0 = 9.75 \cdot 10^{-8} \text{ g/cm}^3$  and  $p_0 = 5.86 \cdot 10^4 \text{ dyn/cm}^2$ . From this the initial magnetic field strength is  $B_{z,0} = 1214 \text{ G}$ .

The equilibrium state constructed this way is perturbed by a sinusoidal oscillation in  $v_x$  at the lower  $z$ -boundary ( $z = 0$ ). Assuming that the whole  $z = 0$  plane is disturbed we write

$$v_x(x, y, z = 0, t) = \hat{v} \sin(2\pi t/P) \quad (12)$$

where  $\hat{v} = 2 \text{ km/s}$  is the amplitude and  $P = 75 \text{ s}$  is the period of the disturbance. The periodic driver specified by (12) gives rise to MHD waves propagating along the flux tube. The lower  $z$ -boundary is otherwise assumed to be a rigid wall for the flow, ie.  $v_z = 0$  and the derivative of  $\rho$ ,  $e$ ,  $v_y$ , and  $B_z$  with respect to  $z$  vanishes. The transverse components  $B_x$ ,  $B_y$  of the magnetic field change its sign by reflection at  $z = 0$ . Note that we do not explicitly specify the magnetic field as a function of time similar to  $v_x$ . Thus, the magnetic bundle does not follow the attached  $x$ -motion and the frozen-in condition is violated at this boundary. Nevertheless, the computational domain excluding the plane  $z = 0$  remains divergence free due to the numerical scheme used. In particular, there is no divergence transported into it. Instead, the boundary conditions are in such a way that the tube cross section at  $z = 0$  is identical to that just above which is subject to the backreaction of the surrounding gas. We find this type of boundary condition more relevant for our problem than keeping the cross section circular at  $z = 0$  throughout the evolution in conjunction with the frozen-in assumption. Latter would mean that the layer  $z = 0$  is artificially unaffected by the outer medium which we believe to be rather unrealistic. The best choice of boundary conditions would be to deal with a model of the excitation itself which is, however, beyond the scope of this paper.

The prescribed velocity  $v_x$  cannot be compared with the velocity at which mass elements move as a whole in a classical *thin* flux tube. So,  $\hat{v}$  does not define the velocity amplitude of the displaced mass elements. In our case,  $v_x$  just excites internal body waves with an a priori unknown amplitude.

At the top ( $z = 1000$ ), a simple outflow boundary condition is adopted. For the lateral boundaries of the basic domain, periodic boundary conditions are used.

Like in Paper I, we apply a nested grid strategy to take care of both an ‘accurate’ description of the internal motions of the tube as well as of the propagation of an external acoustic wave generated by the tube/environment interaction. Here, ‘accurate’ means that the diameter of the tube will be represented by about 20 grid points independent of the tube’s radius. To retain the numerical resolution inside the tube for a fixed size of the basic computational domain this means that even more nested grids must come in use when the radius is decreased. We performed calculations for three different radii, namely  $R_0 = 50, 25, 12.5 \text{ km}$  (referred in the following as  $C_{50}$ ,  $C_{25}$ , and  $C_{12.5}$  case). For this a 3-, 4-, or 5-level grid system is used, respectively. Perpendicular to the tube axis, the nesting of grids looks as shown

in Fig. 2. In all cases, the basic physical domain (on the coarsest grid) is given by  $-1000 < x, y < 1000$  and  $0 < z < 1000$  measured in units of km. Some properties of each grid level are summarized in Table 1.

The set of Eqs. (3)–(8) is solved numerically with the code NIRVANA – a finite difference multiple nested grid code for 3D MHD. It is based on the method proposed by Stone & Norman (1992ab) but in addition to that has implemented a multiple nested grid algorithm to allow for a grid refinement. The basics of the refinement technique can be found in Berger & Olinger (1984) and Berger & Colella (1989). Its use in radiation hydrodynamical problems is discussed by Yorke & Kaisig (1995), and in magnetohydrodynamical flows by Ziegler & Yorke (1997).

Finally, some remarks about the computational effort of this investigation: Especially, the 5-level grid calculation is expensive in CPU time. About 130 h were necessary on a Cray supercomputer for the run  $C_{12.5}$ . Nevertheless, this time is much less than the time required for a comparable single grid calculation assuming the same spatial resolution as the finest grid in our nested grid calculation. In the single grid case an enormous number of grid points, namely  $2 \cdot 10^9$ , and a factor  $\approx 2000$  more CPU time would be needed to do such a calculation. This is by far beyond what is at present possible even with the best computers.

### 3. Numerical calculations

We performed numerical calculations for different flux tube radii. In all calculations, the thermal properties of the flux tube and those of its environment were kept fixed. The calculations can then be characterized by a single parameter eg. the thickness parameter  $\alpha$ . Characteristic wave speeds  $c_S$  and  $c_A$  occurring in the problem are the same in all cases. To estimate the wavelength  $\lambda$  of the excited MHD waves, we take the tube speed

$$c_T = \frac{c_S c_A}{\sqrt{c_S^2 + c_A^2}} \quad (13)$$

as approximate phase velocity (at least for longitudinal tube waves; Paper I, Edwin & Roberts 1983), where the sound speed  $c_S$  is given by  $c_S = (\gamma p_0 / \rho_0)^{1/2} = 10 \text{ km/s}$  and the Alfvén speed  $c_A = B_{z,0} / (4\pi \rho_0)^{-1/2} = 11 \text{ km/s}$ . Thus, one expects with  $P = 75 \text{ s}$  a wavelength of 550 km. Three different flux tubes with thickness  $\alpha = (2\pi/\lambda)R_0 \simeq 0.6, 0.3, 0.15$  corresponding to the cases  $C_{50}$ ,  $C_{25}$ , and  $C_{12.5}$  mentioned earlier are discussed. We start the numerical experiments with a geometrically thick flux tube ( $\alpha \simeq 0.6$ ) and move into the regime of geometrically thin tubes ( $\alpha \simeq 0.15$ ). Our discussion is focused on the resulting geometrical structure of the flux tube and the excited wave pattern inside and outside the tube. Special attention is drawn to the tube/environment interaction which may lead to cross-sectional deformations of the flux tube. If these deformations turn out to be strong, the application of the TFA would become senseless for these cases. We mention in this context that the TFA has often been applied in the literature for wave propagation studies in the solar atmosphere under very similar conditions as regarded here.

### 3.1. Flux tube dynamics

#### 3.1.1. Case $C_{50}$

Similar to the results obtained in Paper I, we find an external sound wave which has an appearance in space characteristic for the transverse excitation. This external acoustic field is a consequence of the interaction between the tube surface and the surrounding gas. The latter is compressed by displacements of the tube which give rise to fluctuations. These fluctuations propagate into the nonmagnetic environment carrying various amounts of wave energy. Because there is no direct excitation of sound waves from the periodic driver, the energy fed into the external acoustic field is taken solely from the tube motions. This inevitably leads to a damping of internal waves due to energy conservation. The amount of energy loss from the tube depends on the strength of interaction. Leakage rates by ‘radiation damping’ are quantitatively estimated as a function of the thickness parameter in a separate section.

A snapshot of the evolution is presented in Fig. 3 given at a time  $t = 102$  s. At this time, the footpoint disturbance has travelled about 1.5 wavelength along the tube. Only slices through the computational domain of the innermost grid (level-2 grid in Table 1) are presented. The left panel shows the plane  $y = 0$  while on the right panel several cross sections are given at different heights. In both figures, the projected velocity fields are shown and a single (solid) contour line defined by  $|\mathbf{B}| = B_{z,0}/2$  is displayed to visualize the flux tube surface. Generally, the evolution and excited motions are quite similar to the  $\beta = 1$  case of Paper I. The only difference arises from the period of oscillation which here was chosen as 75 s compared to 50 s in Paper I. This leads to waves with longer wavelength.

We now summarize the basic results. A well-defined transverse wave propagates upwards as clearly seen in the plane  $y = 0$  but also in the sequence of cross-sections. This wave is confined to the interior of the flux tube, thus representing a body wave. The wavelength can be estimated from Fig. 3 to be about  $\lambda \approx 500$  km consistent with our estimate given above. The wavelength can also be measured from Fig. 4 which shows the  $z$ -profile of the  $v_x$ -component (solid line), averaged over the tube cross section. In addition to the transverse wave which directly results from the footpoint perturbation, a longitudinal internal wave-like motion is observed. It can be identified in Fig. 3 by recognizing the variation of the  $v_z$ -component with height. The corresponding averaged quantity is shown in Fig. 5. Note that for a fixed height,  $v_z$  changes its sign when going from the ( $-x$ ) side (backward side) to the ( $+x$ ) side (forward side) of the tube which is the manifestation of a nonaxisymmetric velocity structure in  $(x, z)$ -planes. We suggested in Paper I, that this nonaxisymmetric appearance probably results from the resistance of the tube plasma to transverse accelerations: A gradient in total pressure across the tube develops triggered by the transverse motion and gives rise to compressions and rarefactions in  $z$ -direction. There is a phase difference of approximately  $\pi$  between both sides. A compression of the backward side corresponds then to a rarefaction on the forward side and vice versa. This nonaxisymmetric velocity pattern can-

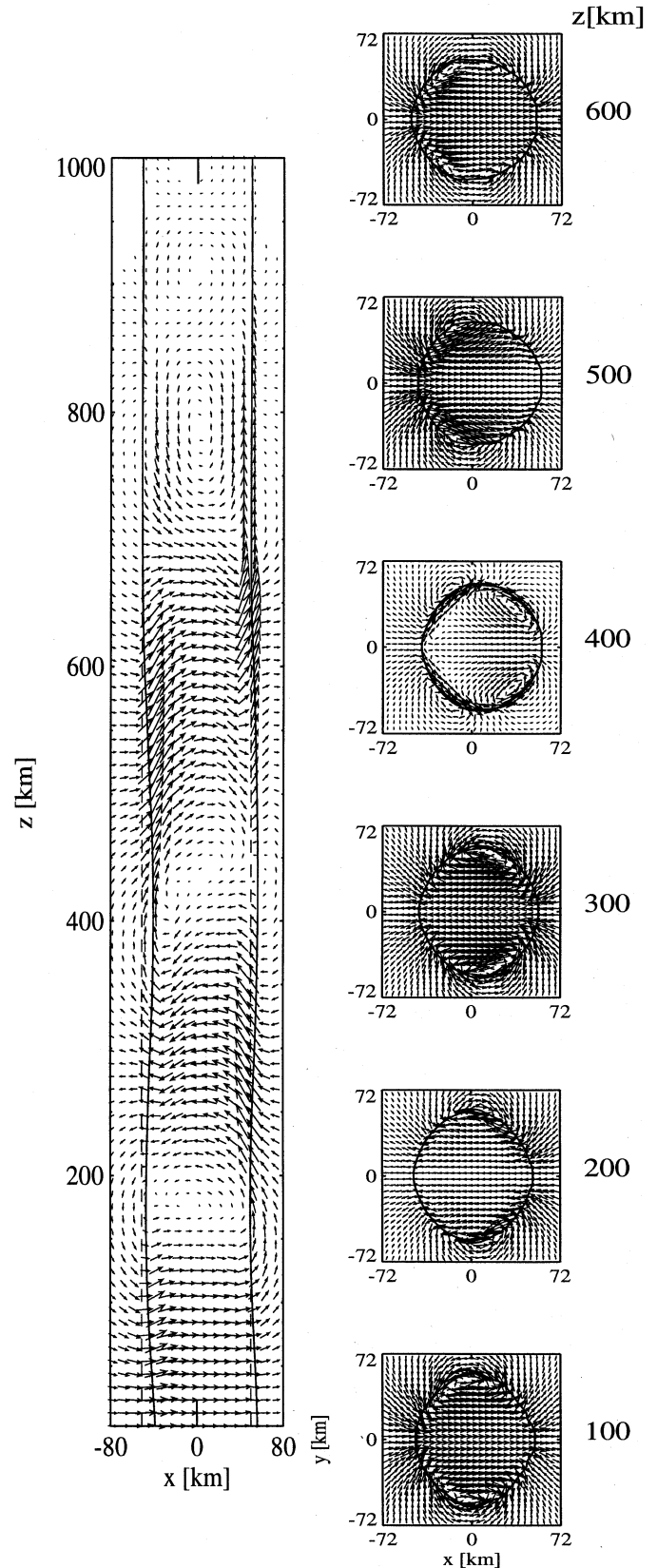


**Fig. 3.** Slices through the computational domain: the plane  $y = 0$  (left) and a sequence of cross sections perpendicular to the  $z$ -axis (right) is shown.  $v_{max} = 1.20$  km/s (0.46 km/s) for the left (right) plot.

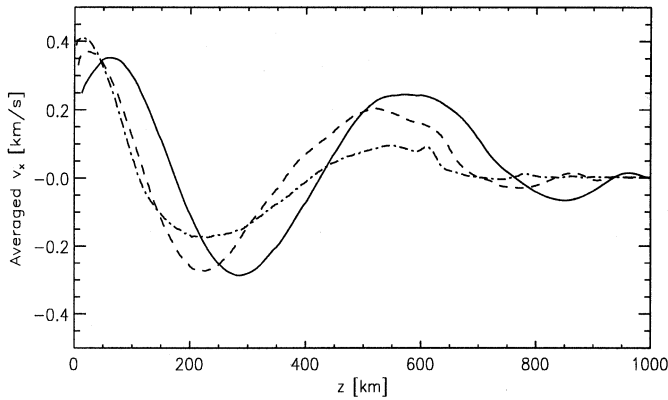


**Fig. 4.**  $z$ -profile of the transverse velocity component  $v_x$  averaged over the tube cross section. The cases  $C_{50}$  (solid),  $C_{25}$  (dashed), and  $C_{12.5}$  (dash-dotted) are shown.

not be explained within the theory for ideally *thin* tubes. Its a phenomenon due to the true 3D structure of the magnetic tube suppressed in *thin* flux tubes. Note the turnover in the velocity profile at  $(x, z) \approx (50, 650)$  km which is likely to be an initial switch-on effect.

A quite distinctive motion is observed in a narrow layer of  $\approx 15$  km around the tube boundary which separates the internal body wave from the flow outside (see the cross sections in Fig. 3). In particular, note in the displayed cross-section the existence of two pairs of vortices at  $z = 400$  km rotating clockwise and counterclockwise around the  $z$ -axis. The boundary layer flow may be interpreted as a transverse surface wave propagating in positive  $z$ -direction and accompanying the internal body waves.

The interaction of the flux tube with the environment leads to a small but visible distortion of its cross section. The magnetic field bundle is compressed in  $x$ -direction (the direction of perturbation) giving the appearance of a more oval shape most prominent at lower heights.

### 3.1.2. Case $C_{25}$

Fig. 6 displays the velocity structure excited in a flux tube with radius  $R_0 = 25$  km half that of case  $C_{50}$ . The time of evolution is  $t = 99$  s. The figures shown correspond to those in Fig. 3. Compared to the previous case, the cross section of the tube is much more deformed which indicates a stronger interaction between the flux tube and the ambient medium. Recall that the  $z = 0$  plane in all three tube cases is excited with the same velocity amplitude. This constitutes a much larger excitation relative to the tube diameter here. The stronger interaction is also perceptible in the energy leakage rate which is a factor  $\approx 2.5$  higher than in the  $C_{50}$  case (see Sect. 4.2 for more detail). Up to height  $z \approx 300$  km, the tube is considerably compressed in the direction of perturbation and somewhat stretched perpendicular to it. For the ratio of major to minor axis of the magnetic bundle one gets a value of  $\approx 2$ . However, compared to the thicker tube,

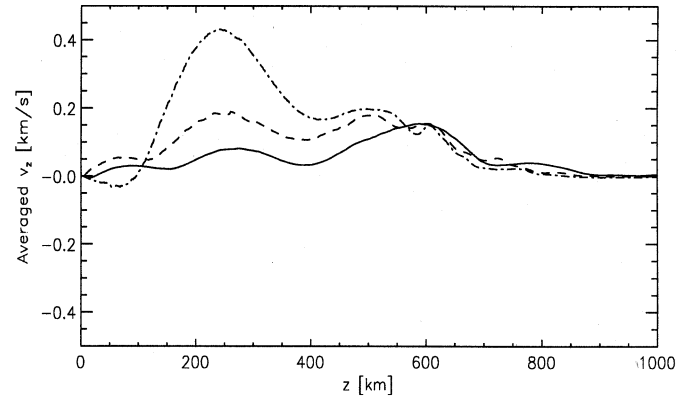


**Fig. 5.** Same as Fig. 4, however, for the vertical velocity component  $v_z$ .

surface phenomena are less striking giving the appearance of a more continuous velocity transition at the tube surface (cf. Fig. 3 and 6 at  $z = 400$  km).

Two types of external forces act on the flux tube which are completely different in physical nature. These are the drag force and ‘acceleration force’. The drag force is a viscous force depending on the tube velocity relative to the external fluid. Because we are dealing with inviscid fluids, the drag force has been ignored in our calculations. Thus, the feedback of the external medium is exclusively due to acceleration reaction.

In contrast to the drag force, the acceleration force only occurs when the tube is accelerated. This kind of backreaction may be understood as a result of an asymmetry in the pressure distribution developing between the backward and forward side during the acceleration. In case of a circular cross section and assumed external potential flow the effect can be described in terms of an increase of inertia of the tube as was first introduced by Spruit (1981a) in the TFA theory. However, as shown here in our  $\beta = 1$  case, the assumptions of a circular cross section and potential flow are too restrictive so that concerning our calculations such a simple description would not be justified under general circumstances.

At first sight it looks surprising that the geometrically thinner tube suffers larger deviations from the ideally *thin* flux tube state than the thicker one does. This means that geometrically thin tubes are not necessarily *thin* in the sense of the TFA theory which has often been assumed to be trivially true. We attribute this contradictory result to the fact that thinner tubes are less inert than thicker ones. Since the driving force is identical for all our flux tube models, cross-sectional mass elements of the thinner tube experience a higher acceleration. Thus, the backreaction force of the environment due to ‘acceleration reaction’ is enhanced in thinner tubes. A very important point noteworthy to recall here is that we used the same numerical resolution in all cases due to the way our experiments has been set up. Therefore, this result is definitely not caused by non-comparable numerical representations.

The excited wave pattern looks similar to that of the previous case but the velocity structure is more complex. Because

of the deformations, the tube plasma moving eg. in positive  $x$ -direction is deflected giving rise to a significant internal  $v_y$ -component which was less important in the case  $C_{50}$ . As a consequence of the deviations from cylindrical geometry, the wave properties, eg. the phase velocity, are modified relative to those in  $C_{50}$  (and even more so relative to the modes propagating in a circular cylinder). This is due to the fact that the tube displaces now a larger external volume relative to the internal volume.

### 3.1.3. Case $C_{12.5}$

Our third calculated flux tube model with a tube radius of  $R_0 = 12.5$  km which corresponds to a thickness parameter  $\alpha \simeq 0.15$  shows the most spectacular behaviour. Like in the other cases, the structure of the velocity and the tube boundary is monitored (Fig. 7). We show slices on the level-3 grid ( $x = 0$  plane) and level-4 grid (cross sections) taken at a time  $t = 96$  s. Unfortunately, these two-dimensional plots give only a poor impression of the true 3D structure. When viewed in 3D, the topology of the magnetic field of the flux tube might be imagined as a tree trunk which is almost split at lower heights.

On average, we can still identify a transverse body wave. Its velocity amplitude, however, is significantly damped when propagating upwards (see Fig. 4). The horizontal motion associated with the body wave leads to the appearance of a plume of external material into the tube which creates strong displacement flows in the tube. At the bottle-neck of the tube ( $z \approx 200 - 300$  km), where an almost complete separation into two counterrotating legs occurs, strong vertical velocities arise. Magnitudes of these velocities are found to be twice as large as for the  $v_x$ -component. In Fig. 5, the corresponding averaged  $v_z$ -profile shows a clear maximum at this height. Note that vertical velocities are larger at the forward side of the tube than backwards which is indicated by the peak in Fig. 5.

Although the flux tube with  $R_0 = 12.5$  km is the thinnest one considered ( $\alpha$  smallest), it shows a behaviour at variance to that of a perfect *thin* tube. All wave quantities are far away from a representation by a single space coordinate  $s$  (a curve parameter) like in a *thin* flux tube. Gradients perpendicular to the tube axis develop which cannot be neglected compared to those occurring along the axis (see eg. the velocity structure at  $z = 400$  km). Thus, higher-order moments in an expansion of the form (1) become important which invalidate a description within the framework of the TTFA. The development of transverse gradients obviously is a consequence of the even more intensified interaction with the surrounding gas. In the TFA theory it is assumed that this interaction does not have an influence on the shape at all and, therefore, on the dynamics of the internal plasma. Here, the interaction process is found to be of essential importance.

The strong deformations of the cross section are accompanied by a very large loss of tube energy by leakage into the nonmagnetic environment by radiation of acoustic waves. As discussed in more detail in the following section more than 75% of the tube wave energy is fed into the external wave. Consequently, the energy flux carried by the tube body waves is con-

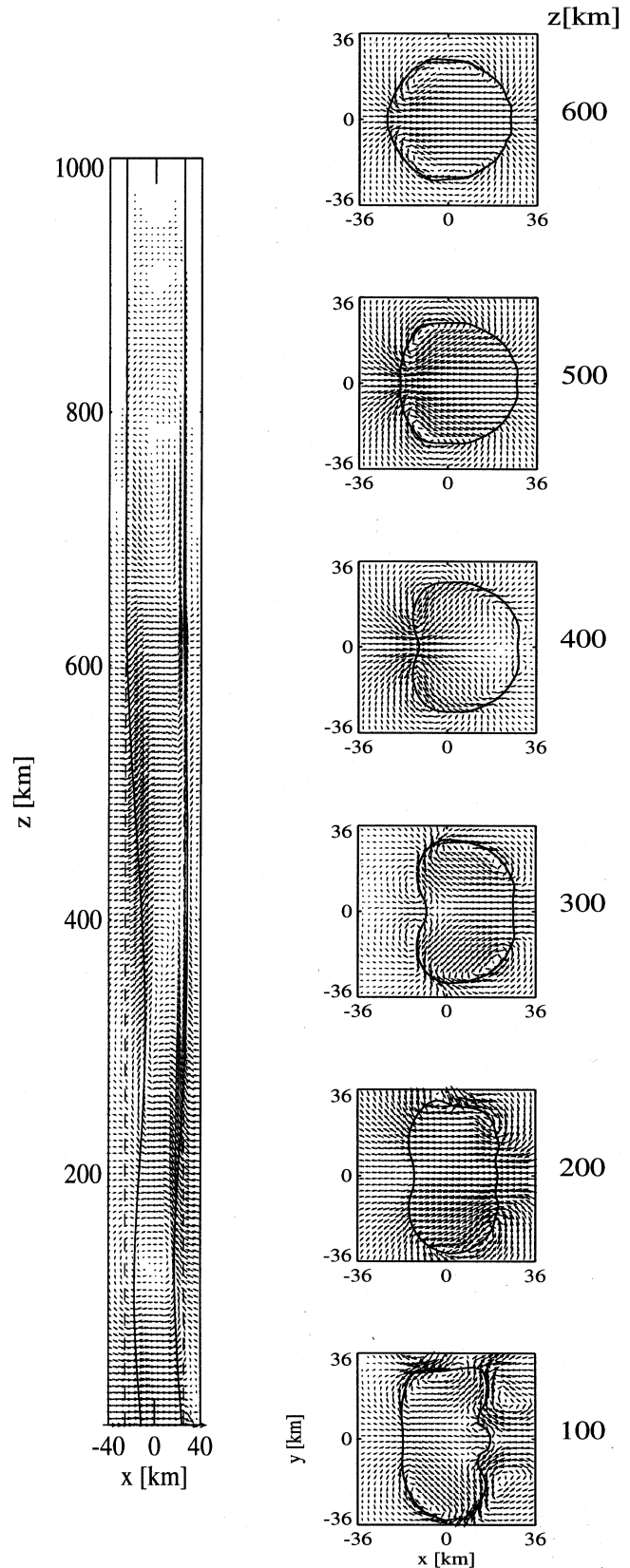


**Fig. 6.** Same as Fig. 3 for  $R_0 = 25$  km, however,  $v_{max} = 1.11$  km/s for the left plot respective  $v_{max} = 0.65$  km/s for the right plot.

siderably reduced at greater heights which can be seen by the drastic decay of the velocity amplitude in Fig. 4 (dash-dotted line).

### 3.2. Energy leakage

The loss of tube wave energy to the surroundings by acoustic radiation is seen to be inherently coupled with the strength of interaction between the flux tube and the ambient medium. A stronger interaction means high energy losses and vice versa. We have calculated energy leakage rates (or damping rates) expressed by  $D(t)$  using the formulae given in Paper I. Relevant wave energies are summed up inside and outside the tube to define a leakage rate according to

$$D(t) = \frac{\langle E_{tot}^e \rangle}{\langle E_{tot}^e \rangle + \langle E_{tot}^i \rangle} \quad (14)$$

where  $\langle E_{tot}^e \rangle$  and  $\langle E_{tot}^i \rangle$  denote the total wave energies outside and inside the tube integrated over time. Defined in this manner,  $D(t)$  quantitatively describes the amount of energy which on average leaks out of the tube.

For the calculated cases  $C_{50}$ ,  $C_{25}$ , and  $C_{12.5}$ , the time evolution of  $D(t)$  is illustrated in Fig. 8. After an initial phase of adjustment, the tube with  $R_0 = 50$  km quickly reaches a stationary state with a leakage rate of  $D \approx 0.2$ . This happens after  $t \gtrsim P/2$ . In the case  $C_{25}$ , the leakage rate monotonically increases up to a maximum value of  $\approx 0.75$  at  $t \approx 0.7P$  and then falls down to  $D \approx 0.5$  at the end of the calculation. Yet, most probably it has not quite reached its final stationary value which would be expected for  $t \gg P$ .

The behaviour of the case  $C_{12.5}$  is quite similar to that of  $C_{25}$ . However, due to the stronger tube/environment interaction the thinner tube leaks relatively more energy than the thicker one does. Moreover, the  $C_{12.5}$  curve falls down less steeply yielding a final value of  $D \approx 0.8$ . Like in the case  $C_{25}$ , stationarity is not reached. From all this we conclude that energy loss from the tube to the ambient medium monotonically increases with decreasing tube diameter. This has to be confronted with the TFA which totally ignores energy losses. Up to now no attempt has been made to include radiation damping within the concept of the TFA, although it may be possible in principle. As seen here, energy leakage in transversely excited geometrically thin flux tubes is an important effect which cannot be ignored.

## 4. Conclusion

Our numerical computations in 3D geometry were performed to gain more insight in the applicability of the TFA for geometrically thin flux tubes with moderate magnetic field strength ( $\beta = 1$ ) when excited by means of a periodic transverse driver. The basic findings of these computations are:

1. Within the framework of our model, we conclude that the TFA would get worse if applied to geometrically thin flux tubes i.e. flux tubes with a small thickness parameter  $\alpha$ . For

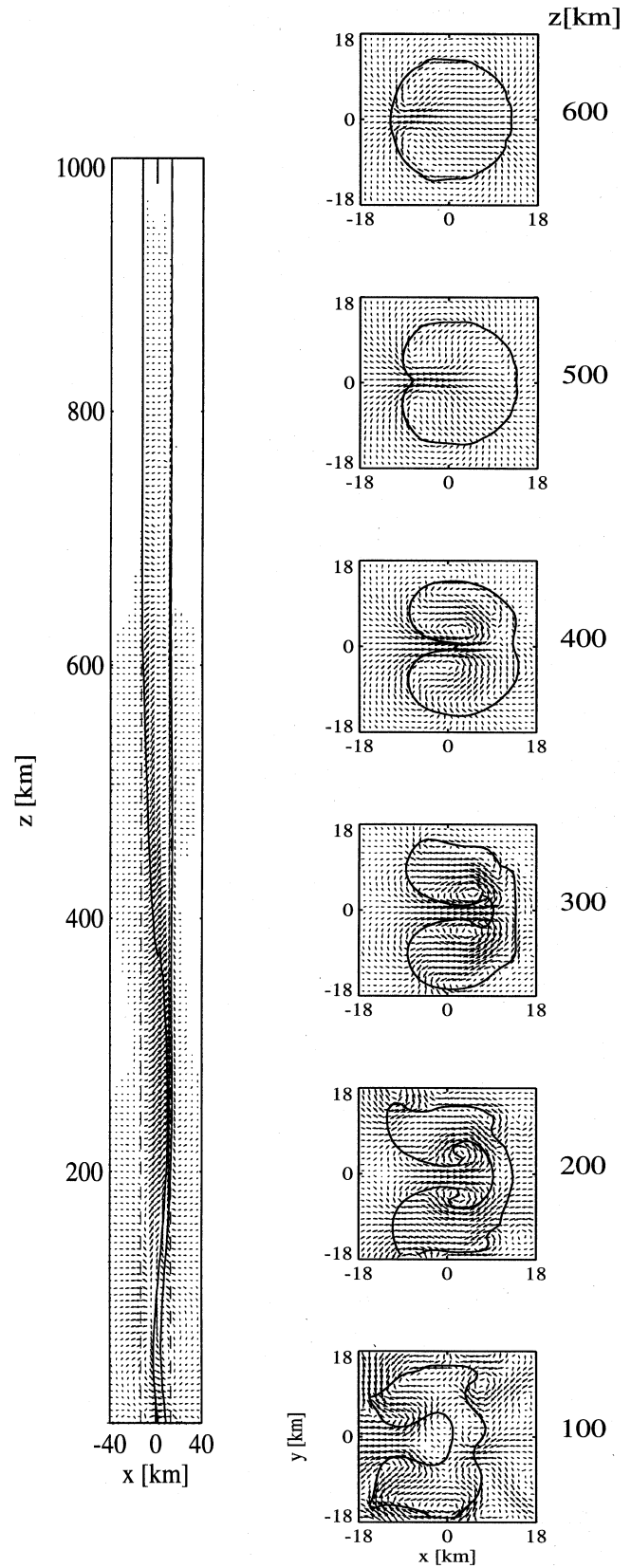
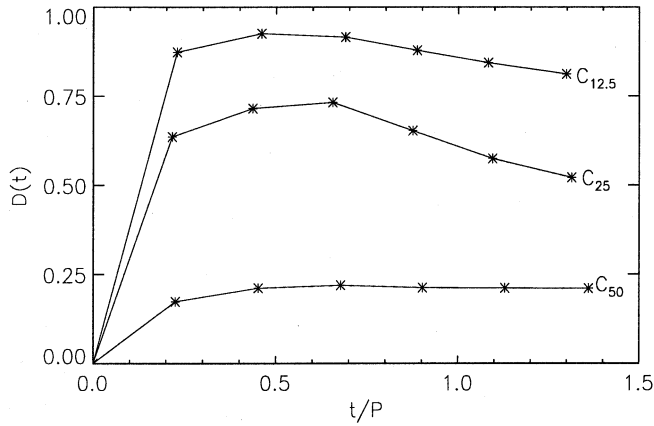


Fig. 7. Same as Fig. 3 for  $R_0 = 12.5$  km, however,  $v_{max} = 0.99$  km/s for the left plot respective  $v_{max} = 0.74$  km/s for the right plot.



**Fig. 8.** Energy leakage rate  $D(t)$  as a function of dimensionless time  $t/P$  for the calculated cases  $C_{50}$ ,  $C_{25}$ , and  $C_{12.5}$ . Stars denote the actually computed values which are connected by lines.

the validity of the TFA it is therefore not sufficient to suppose just geometrical thinness of the tube. The main reason for that is the following: Thinner flux tubes while less inert when subject to a prescribed driving mechanism, experience stronger backreaction forces than corresponding thicker ones. Relatively large variations of all wave quantities across the tube occur which do not justify a description as ideally *thin* flux tube.

- For excitations where more external volume relative to the tube volume is displaced, the deformations of the cross sections become larger and the dynamics of the internal plasma is more affected. This would imply that the TFA is restricted to only very small transverse excursions of the tube. In the  $C_{12.5}$  case we found an almost complete split-up of the tube in two counterrotating legs (cf. Fig. 7). Larger excitation amplitude or alternatively a weaker magnetic field would probably lead to a complete splitting of the tube at lower heights with the magnetic field taking on a fork-like topology.
- Tube deformations are accompanied by high energy losses to the surrounding gas by radiating away acoustic waves. Energy leakage rates range from  $\approx 0.2$  for the flux tube with a radius of 50 km up to  $\approx 0.8$  for the tube with radius 12.5 km. Thus, the energy loss increases monotonically with decreasing tube diameter.
- An interesting question concerns the role of the magnetic field strength which we did not vary in our calculations. We believe that low  $\beta$ -tubes (with stronger magnetic fields) are stabilized against lateral deformations whereas high  $\beta$ -tubes (with weaker magnetic fields) experience an even stronger interaction with the ambient gas. A relatively weaker magnetic field means that the flux tube can more easily be compressed by the surrounding flow. Thin high  $\beta$ -tubes are therefore still worse candidates for the applicability of the TFA. On the other hand, very low  $\beta$ -tubes may be good candidates.

- A quite different situation may exist when tube waves are excited purely longitudinally which we also have not considered. In this case, tube displacements lead to an interaction with the surroundings because of compressions and rarefactions analogous to that in a pulsating pipe. In contrast to transverse shaking, however, shape deformations are usually moderate and axially symmetric. Therefore, the internal plasma would not be influenced much, i.e. transverse gradients would be small compared to longitudinal ones. For this reason, we speculate that the TFA may be much more accurate in cases of longitudinal wave excitation even for tubes with thickness parameter  $\alpha \approx 1$ .

*Acknowledgements.* The calculations were performed on a CRAY supercomputer at the Rechenzentrum der Universität Stuttgart. We gratefully acknowledge financial support of the Sonderforschungsbereich SFB 328 of the Deutsche Forschungsgemeinschaft (DFG).

## References

- Berger M.J., Colella M.J., 1989, JCP 82, 64  
 Berger M.J., Olinger J., 1984, JCP 53, 484  
 Cheng J., 1992, A&A 264, 243  
 Choudhuri A.R., 1990, A&A 239, 335  
 Edwin P.M., Roberts B., 1983, SP 88, 179  
 Fan Y., Fisher G.H., McClymont A.N., 1994, ApJ 436, 907  
 Ferriz-Mas A., Schüssler M., Anton V., 1989, A&A 210, 425  
 Ferriz-Mas A., Schüssler M., 1989, Geophys. Astrophys. Fluid Dyn. 48, 217  
 Moreno-Insertis F., Schüssler M., Ferriz-Mas A., 1996, A&A in press  
 Osin A., Volin S., Ulmschneider P., 1997, A&A submitted  
 Roberts B., Webb A.R., 1979, SP 64, 77  
 Schramkowski G.P., Achterberg A., 1993, A&A 280, 313  
 Spruit H.C., 1981a, A&A 98, 155  
 Spruit H.C., 1981b, A&A 102, 129  
 Stone J.M., Norman M.L., 1992a, ApJS 80, 753  
 Stone J.M., Norman M.L., 1992b, ApJS 80, 791  
 Ulmschneider P., Zähringer K., Musielak Z.E., 1991, A&A 241, 625  
 Vernazza J.E., Avrett E.H., Löser R., 1981, ApJS 45, 635  
 Yorke H.W., Kaisig M., 1995, CPC 89, 29  
 Ziegler U., Ulmschneider P., 1997, A&A, submitted  
 Ziegler U., Yorke H.W., 1997, CPC, 101, 54